ARTICLES

Fluorescence and Resonance Raman Spectra of the Aqueous Solvated Electron

Michael J. Tauber and Richard A. Mathies*

Department of Chemistry, University of California, Berkeley, California 94720

Received: June 8, 2001; In Final Form: October 2, 2001

Fluorescence and resonance Raman spectroscopy are used to probe the solvent structure and dynamics of the aqueous solvated electron. Electrons are generated by 218 nm photolysis of iodide or ferrocyanide, and spectra are obtained with 532 or 683 nm probe wavelengths. Strong resonance enhancement of the water Raman librational bands and intramolecular bend and stretch are observed, and the frequencies of the enhanced intramolecular modes are significantly downshifted from the corresponding bands in pure water. The resonance Raman enhancements show that the s→p transition of the aqueous solvated electron is coupled to both inter- and intramolecular solvent modes. A broad fluorescence emission underlying the Raman features and extending past 1600 nm into the near-IR is observed due to the solvated electron. The fluorescence quantum yield in H_2O is $\sim 7 \times 10^{-7}$ and it increases 1.4-fold in D_2O. A Strickler−Berg analysis of the absorption and emission spectral profiles indicates a near-IR radiative lifetime of ∼40 ns. Effective fluorescence lifetimes based on the 720−1600 nm emission quantum yields and radiative lifetime are ∼30 fs for the electron in H_2O and ∼40 fs in D_2O. The isotope effect and breadth of the emission indicate that, upon photoexcitation, >1 eV of solvent relaxation occurs primarily along rotational coordinates and is likely much more rapid than internal conversion to the ground s-state.

1. Introduction

The apparent simplicity of the solvated electron makes it an ideal solute for studying solvation in polar and nonpolar solvents. In particular, the discovery of the aqueous solvated electron[1] has inspired many experimental and theoretical studies. Absorption spectra of hydrated electrons support a cavity model analogous to the description of electrons solvated in ammonia, amines, alcohols, and other solvents.[2] ESR spectra of the electron trapped in a low-temperature aqueous glass indicate a distance of 2.1 Å between the charge center and the nearest protons[3,4] in close agreement with the cavity radius of the ground s-state determined in computer simulations.[5] The relaxation of electrons after excitation to the lowest (2p) excited-state manifold has been probed by femtosecond transient absorption spectroscopy. Recovery of the ground-state bleach and an absorption in the near-IR exhibit a fast ∼30−80 fs Gaussian component[6,7] followed by 190−300 fs and ∼1 ps exponential decays.[6−10] The absorption transients have been interpreted in terms of two general models: in one, rapid ≤300 fs p-state solvation precedes a 300 or 1000 fs nonadiabatic transition,[6−8,11] and in another an ultrafast ∼50 fs or ∼190 fs p→s crossing precedes ∼1 ps cooling on the ground state.[7,9,10] Kinetics observed in the femtosecond transient absorption experiments of photoinjected electrons support the slower nonadiabatic transition proposed in the first model.[12,13]

Recent semiclassical molecular dynamics (MD) simulations have contributed significantly to the interpretation of the transient absorption experiments and to our general understanding of both static and dynamic characteristics of the aqueous solvated electron.[11,14−22] The simulations attribute the width of the absorption spectrum to an ∼6000 cm^{-1} splitting of the three p-like excited states and to rapid solvent fluctuations that broaden each s→p subband by ∼3000 cm^{-1}.[22] The simulations specific to transient absorption experiments present a model of fast spectral diffusion and solvation of the p-state, followed by slow ∼1 ps nonadiabatic relaxation.[11] Another finding of the MD simulations is an enormous Stokes shift[11,14] which is analogous to the large p-state relaxation found in the application of semicontinuum dielectric theory to the solvated electron in ammonia and water.[23,24] The predicted fast evolution of the excited state and dramatic Stokes shift spurred our interest in measuring resonance Raman and fluorescence emission spectra of the solvated electron to obtain more information about the structural relaxation dynamics.

Resonance Raman spectroscopy is an ideal technique for probing the coupling of an electronic transition to Franck−Condon active vibrations of a chromophore and revealing the inertial dynamics along these structural coordinates after photoexcitation.[25] Can *solvent* vibrational modes show Raman enhancement upon resonant excitation of a solute molecule? Vibronic coupling of this type has never been observed via resonance Raman spectroscopy of molecular solutes,[26,27] but the solvated electron presents a special case because unusually strong association between the solute (electron) and solvent is expected. The observation of an analogous vibronic response in the solid state was demonstrated in a pioneering study of F-centers (the solid-state analogue to solvated electrons) which employed near-resonance Raman spectroscopy to reveal the coupling between trapped electrons and phonons of the sur-

* To whom correspondence should be addressed. E-mail: rich@zinc.cchem.berkeley.edu. Phone: (510) 642-4192. Fax: (510) 642-3599.

10.1021/jp012184p CCC: $20.00
Published on Web 11/14/2001

rounding crystal lattice.[28] Attempts at finding Raman bands of the solvated electron in liquid ammonia were unsuccessful,[29−31] and the *resonance* Raman spectrum of any solvated electron system remains an outstanding problem.

The measurement and analysis of the fluorescence spectra in tandem with the resonance Raman cross-sections have led to an improved understanding of the excited-state dynamics of a number of molecular systems.[32−37] Fluorescence spectroscopy can provide direct information about the evolution of the excited-state far outside the Franck−Condon region. Measurement of the fluorescence spectrum and quantum yield of the solvated electron in particular opens the possibility of elucidating critical features of the excited state, such as the lifetime, the rate and magnitude of relaxation outside of the Franck−Condon region, and the total reorganizational energy. Any aspect of solvation measured for this system is especially valuable, since the solute (electron) lacks intramolecular structure and allows definite assignment of the dynamics to the solvent. By contrast, studies of molecular solutes have suffered from the problem of differentiating the intramolecular response from the solvent response, especially on the fastest time scales probed by time-resolved fluorescence and photon echo experiments. [34,38−41]

We present here the first resonance Raman and fluorescence spectra of the electron solvated in H_2O and D_2O. Strong enhancement of the water librational band and intramolecular bend and stretch are observed, along with significant downshifts in the vibrational frequencies of the bend and stretch. This report is focused on the extremely broad fluorescence emission measured out to 1.6 μm, from which we derive an effective radiative lifetime of the excited state. An isotope-dependent fluorescence quantum yield of $\sim 10^{-6}$ is measured and used to establish a near-IR fluorescence lifetime of ~30 fs. The weak emission and fast decay time are discussed in terms of two possible mechanisms: an ultrafast internal conversion and an ultrafast dynamic Stokes shift.

2. Materials and Methods

2.1. Sample and Flow System. Aqueous solvated electrons were produced by 218 nm photolysis of dilute ferrocyanide or iodide solutions through the charge-transfer-to-solvent process.[42,43] Ferrocyanide was found to be advantageous because of the greater yield of photogenerated electrons[44,45] and much lower fluorescence background from the 218 nm pump beam. Dilute aqueous solutions of $Fe(CN)_6^{4-}$ were prepared with reagent-grade potassium ferrocyanide trihydrate (Aldrich). Water was distilled and filtered by a five-stage system (Millipore/MilliQ-Plus) or 99.9% D_2O (Cambridge Isotope Labs). Solutions were recirculated in a flow system using a peristaltic pump and were gravity-driven through a stainless steel jet nozzle and down wire guides with an approximate linear velocity of 1 m/s, forming a sampling region ~200 μm thick and ~2 mm wide. The ferrocyanide concentration (2.5 mM) yielded an optical density of >1 through the jet.[44] Solutions were replaced hourly to avoid buildup of side products.

Solvated electron concentrations averaged along the ~280 μm diagonal path length through the jet were determined by measuring the change in probe transmission through the sample caused by the pump pulse and by using the decadic molar extinction coefficients of the solvated electrons in H_2O or D_2O at λ_{probe}.[46] For the 532 nm probe experiment the average concentration was 0.31 mM ($\Delta OD = 0.065$, $\epsilon_{532} = 7500\ M^{-1}\ cm^{-1}$) from which concentrations of 1.1 mM at the front and <0.05 mM at the rear of the jet are computed. For the scanning experiments using a 683 nm probe, the average solvated electron concentration in H_2O was 0.25 mM ($\Delta OD = 0.13$, $\epsilon_{683} = 18\,400\ M^{-1}\ cm^{-1}$) and in D_2O the result was 0.29 mM ($\Delta OD = 0.16$, $\epsilon_{683} = 19\,600\ M^{-1}\ cm^{-1}$). The slight variations in average electron concentration are attributed to drifts in the pump intensity.

2.2. Laser System. All experiments employed a single Nd:YAG laser (Quanta Ray DCR-2A, 8 ns pulse width, 20 Hz repetition rate) equipped with 2nd and 4th harmonic crystals. The configuration for the 218 nm pump, 683 nm probe experiments is as follows. The collinear 1064, 532, and 266 nm lines were focused into a 0.87 m long Raman shifter filled with 100 psi of H_2. A crystal quartz Pellin-Broca prism was used to disperse all wavelengths and isolate the 218 and 683 nm lines. The delay between pump and probe was ≥10 ns to ensure that electrons were probed in the ground state. The horizontally polarized beams were made collinear with a dichroic beamsplitter and focused with two orthogonal fused silica cylindrical lenses (f.l. 100 and 75 mm) onto the vertical flowing sample jet in a 45° backscattering geometry. Pump spot sizes ranged from 200 to 400 μm wide x 3.5 mm high, and probe spot sizes ranged from 125 to 200 μm wide x 3.2 mm high. The pump was larger than the probe in both dimensions to ensure that the full probed region contained solvated electrons. Pump powers ranged from 1.8 to 2.8 mW. Probe powers were typically 2−6 mW, with a 10% variation in a given experiment. The Raman and fluorescence signals scaled linearly with the probe power over the range 0.3−6 mW.

The probe for the post-resonant experiments was a portion of the 532 nm laser output. The beam was sent through a 20 ns optical delay, which included filters for blocking the other Nd:YAG harmonics and apertures to reduce the divergence and intensity of the beam. The power at the sample was ~2.2 mW (pump) and ~2.3 mW (probe).

2.3. Measurement of NIR Spontaneous Emission Spectra. Emission resulting from 683 nm excitation of electrons solvated in H_2O and D_2O was measured over the visible-NIR spectral range using a PMT with an InP/InGaAs transferred electron photocathode cooled to −80 °C (Hamamatsu R5509-72). The use of gated analogue detection with 20 ns gate width allowed sufficient rejection of the ~90 nA dark current background (bias −1750 V) so that the PMT noise was negligible. The PMT anode was terminated into the 50 Ω input of a 300 MHz preamplifier (Stanford Research SR-445) coupled to a gated integrator/boxcar averager (Stanford SR-250). The exponential average was set to 30 samples (1/*e* time constant 1.5 s). The SR-250 output was read by an A/D board (National Instruments PCI-MIO-16XE−50). A second channel of the A/D board was used to continuously monitor the probe power. A LabView program controlled the scanning spectrometer and voltage readouts of the data acquisition board. The time between readouts was ~3 s, and step sizes were 1 nm/step (720−1000 nm) and 2 nm/step (1000−1700 nm). For scans of ferrocyanide in H_2O, five sets of grouped sequential acquisitions of pump + probe, probe-only, and pump-only were acquired. For ferrocyanide in D_2O, four sets each were acquired.

A single F/4 spectrometer (JY Horiba/Spex 500M) equipped with a gold-coated 600 g/mm, 1.0 μm blazed grating (Richardson Grating Lab) was employed for the scans. Scattered light was collected, collimated, and focused onto the entrance slit with two uncoated fused silica lenses (F/1, f.l. 50 mm, and F/4, f.l. 200 mm). A crystal quartz polarization scrambler (Karl Lambrecht) was positioned several centimeters in front of the entrance slit. For scans from 720 to 1000 nm, two 715 nm long-pass filters (Schott RG-715) were placed between the polariza-

tion scrambler and entrance slit to attenuate the Rayleigh scattering. To avoid possible interference from 2nd-order light over the scan from 1000 to 1700 nm, one of the 715 nm long pass filters was replaced with an 850 nm long-pass filter (Schott RG-850). The 1 mm slit width gave a band-pass of 3.2 nm (11−62 cm^{-1}).

An instrument response curve was obtained from a scan of a calibrated quartz tungsten halogen lamp (GE) in an EG&G 590-20 housing. The light was chopped at 40 Hz, and the detection apparatus was unchanged except for replacement of the gated integrator with a lock-in amplifier (Stanford SR830). Calibrated values of spectral energy irradiance (in $\mu W/cm^2$ nm) provided by the Eppley Laboratory were converted to a corresponding photon count irradiance before these values were used to obtain the instrument response. Any emission spectrum divided by this instrument response maintains a *y*-axis intensity that is proportional to the *number of photons* and is corrected for variation in sensitivity across the window.

The instrument response curve does not correct for chromatic aberrations of the collection lenses since the entrance slit is illuminated differently during the Raman experiment as compared with the scans of the calibrated lamp. We have experimentally estimated the chromatic loss by illuminating a 200 μm vertical wire at the sample point with white light incident at approximately 45°. The diffuse broadband reflection from the wire has a width that is comparable to that of the focused laser beam at the sample point of the scanning Raman experiment, therefore the illumination of the entrance slit is similar in both cases. With this source, a ∼12% increase in signal at 1500 nm was obtained by refocusing the collection lens that had been previously adjusted to optimize collection of 900 nm light (the water Raman stretch wavelength for 683 nm excitation). An approximate linear correction over the range 900−1600 nm is included in the data workup to compensate for this variation in collection efficiency.

2.4. Setup for 532 nm Postresonant Experiments. The detection setup for 532 nm excitation employed a front-illuminated open electrode CCD (Roper Scientific LN/CCD 1024-E/OP/1). The spectrograph was a Spex 500M with a 300 g/mm, 500 nm blazed grating (Richardson). A 515 nm long-pass filter (Schott OG-515) and a 532 nm notch filter (Kaiser Optical) positioned between the polarization scrambler and entrance slit blocked stray pump light and the 532 nm Rayleigh line. The spectral band-pass was ∼85 cm^{-1}. The spectral sensitivity of the detection system was measured with the Eppley calibrated quartz tungsten halogen lamp to obtain a photon count instrument response over the wavelength region 400−980 nm.

2.5. Methods for 218 nm Pump, 683 nm Probe of Acidified I^- Solutions. Dilute I^- solutions were acidified with 0.100 N HCl (Fisher) to achieve H^+ concentrations between 0 and 27 mM. The open vertical jet system was modified so that the acidified solutions contacted only glass, fused quartz, and Viton tubing. A peristaltic pump was employed to force the recirculating solution through a nozzle consisting of a 3 cm length of o.d. 350 μm, i.d. 180 μm fused quartz capillary tubing (Polymicro Technologies). The delay between 218 nm pump and 683 nm probe was 10 ns, and the beams were focused to a circular spot at the sample point. The detector was a back-illuminated CCD (Princeton Instruments PB/UVAR 1100).

2.6. Data Workup. The solvated electron spectra were obtained by the following steps: (1) remove detector baseline offsets and peaks from stray light scattering by subtraction of select pairs of raw spectra; (2) divide by the instrument response; (3) correct for attenuation of bulk water Raman signal due to solvated electron absorption; (4) subtract bulk solution Raman scattering from solvated electron + bulk solution spectrum; and (5) correct solvated electron spectrum for self-absorption. The effects of electron absorption were quantitatively modeled with numerical integrations based on Beer's Law, incorporating the experimentally measured attenuation of the transmitted probe and solvated electron absorption spectrum[46] $\epsilon_{elec}(\lambda)$ as inputs. The results show that the attenuation of Raman scattering from bulk water is due to absorption of the excitation beam traversing the jet (∼10% for 532 nm, ∼20% for 683 nm) and direct absorption of the Raman scattering [0−16% depending chromatically upon $\epsilon_{elec}(\lambda)$]. The probe-only spectrum is adjusted to reflect both these sources of attenuation in step 3 above. Similarly, the minor loss of fluorescence and Raman emission from the solvated electron due to "self-absorption" is compensated for in step 5. Numerical analysis shows that the total attenuation (<20%) of the solvated electron emission is less than the loss of emission from the bulk solution, since the former originates primarily from the front of the jet.

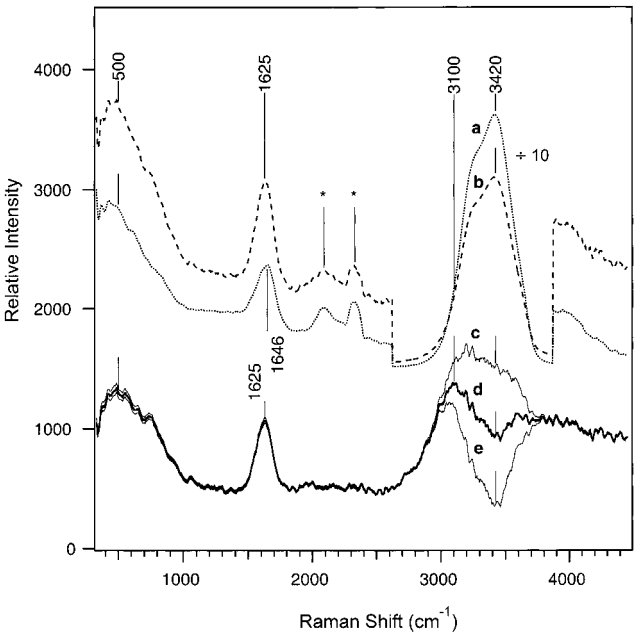

Figure 1. Raman and fluorescence emission spectra of the aqueous solvated electron with 532 nm probe excitation. Probe-only minus background spectrum (a, ···) and pump + probe minus pump-only spectrum (b, - - -) are offset +1500 units and the water stretch signals of both are divided by 10. Minor peaks due to metal-cyanide anions (2055−2135 cm^{-1}) or stray laser light (2335 cm^{-1}) are indicated by an asterisk (*). The lower solid traces are the solvated electron difference spectra where the subtraction coefficients are (c) 0.92, (d) 0.95, and (e) 0.98. Traces (c−e) are not offset; departure from baseline is entirely due to fluorescence from the solvated electron. All spectra have been corrected for the instrument response and spectra (c−e) have been corrected for chromatic self-absorption by the electrons.

3. Results

3.1. 532 nm Raman Probe of $e^-(H_2O)$. The probe-only Raman spectrum of bulk water and dilute ferro/ferricyanide anions is presented in Figure 1a after subtraction of a background spectrum and division by the instrument response. Subtraction of the pump-only spectrum from pump + probe removes most stray laser lines and completely removes the fluorescence contribution due to the pump. This spectrum (b) has spectral features due to bulk water, ferro/ferricyanide, and solvated electrons. Attenuation of emission intensity across the full spectrum due to absorption by the solvated electrons is

shown by a ~25% decrease in the water Raman stretch band at 3400 cm^{-1}. Despite these absorptive losses, the spectrum of water and electrons clearly show *increased* Raman scattering activity at the water librational modes (near 500 cm^{-1}) and intramolecular bending mode (1625 cm^{-1}). Furthermore, the entire background of spectrum b is significantly elevated above the probe-only background (a). Both the enhanced Raman features and the broad fluorescence background are unquestionably present irrespective of how the Raman scattering from the bulk solution is removed.

To obtain a pure solvated electron emission spectrum, we take the difference (spectrum b) − (spectrum a) after compensating for absorption of the bulk water Raman by solvated electrons as explained above. The subtraction must be further optimized to achieve a physically reasonable difference spectrum in the water Raman stretch region from 3200 to 3600 cm^{-1}, presented in Figure 1 as spectra c, d, and e. The bulk Raman scattering has likely been oversubtracted in spectrum e and undersubtracted in spectrum c. Assuming that the fluorescence component varies smoothly across the window, the optimum subtraction is spectrum d. Note that all three difference spectra include correction for self-absorption which varies <6% across the spectral window.

The 532 nm excited solvated electron spectrum d shows strong resonance enhancement in the water librational region ranging from the lowest frequency of accurate spectral correction ~400−1000 cm^{-1}. The shape of the broad band is weighted slightly more toward higher Raman frequency as compared with the bulk water libration. The solvated electron water bend shows a single symmetric peak at 1625 cm^{-1}, downshifted ~20 cm^{-1} relative to the peak frequency in bulk water. A Raman band peaked at ~3100 cm^{-1} is also evident in the water stretch region. Although the peak maximum, breadth, and intensity of this band are sensitive to the details of how the bulk water stretch contribution is subtracted, nonetheless there is undoubtedly enhancement from 2700 to 3200 cm^{-1}.

3.2. Investigation of Raman Water Bend and Fluorescence Intensity. The enhanced water Raman bend and the underlying fluorescence were examined in experiments using a 683 nm probe with both I^- and $Fe(CN)_6^{4-}$ sources. Similar to the 532 nm spectra, the water bend peak of the solvated electron downshifts 33 ± 5 cm^{-1} relative to the bulk water bend (Figure 2, spectra a and e). The fluorescence and bend enhancement are readily apparent. After subtraction of the probe-only bulk water component, the solvated electron bend exhibits resonance Raman intensity ~10 times greater than the Raman intensity of the bulk water bend, *despite the sub-millimolar concentration of electrons*. The observation of fluorescence and Raman enhancement of the bend using ferrocyanide or iodide parent anions and for probe wavelengths that are resonant or post-resonant with the solvated electron provide strong evidence that the solvated electron is the source of both spectral features.

As an additional check of the source of fluorescence and bend enhancement, these two spectral signatures were measured as a function of electron concentration, using H^+ as a scavenger to reduce the initial electron concentration in a predictable way during the ~10 ns delay between pump and probe pulses. The reaction $e^- + H^+ \rightarrow {}^1/_2H_2$ depletes the electrons via pseudo first-order kinetics. Figure 2 inset plots the decay of fluorescence and bend area of the solvated electron as the acid concentration is increased stepwise from to 0.0 to 27 mM. Single-exponential fits to the decays of both spectral features yield an average exponential decay constant of 140 M^{-1}, which corresponds to a second-order rate constant of 1.4×10^{10} M^{-1} s^{-1}. This measured rate constant is within 15% of 1.6×10^{10} M^{-1} s^{-1} which is extrapolated from the established value at zero ionic strength (2.3×10^{10} M^{-1} s^{-1}) by use of the Brönsted-Bjerrum relationship at the average ionic strength of 0.031 molality for these experiments.[47] The agreement of the decay rates strongly supports the conclusion that both the bend enhancement and fluorescence originate from the solvated electron.

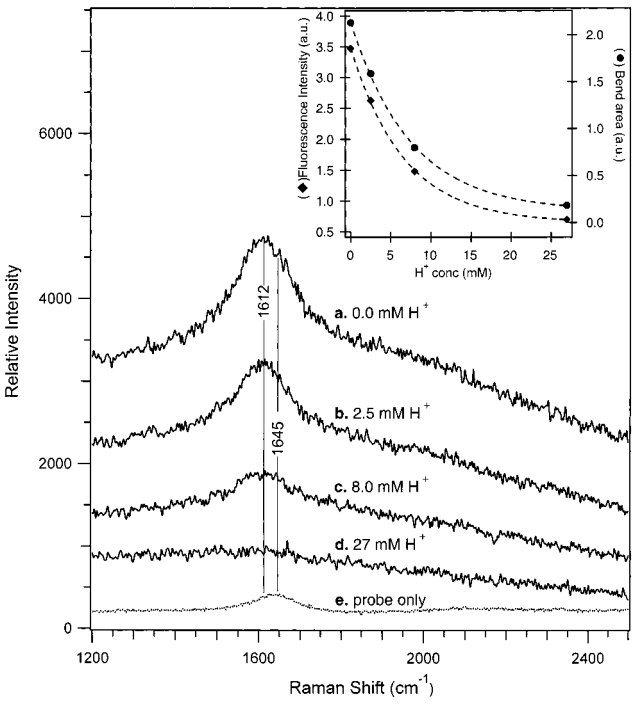

Figure 2. Raman and fluorescence emission (a−d) from the aqueous solvated electron probed with 683 nm excitation ~10 ns after formation. The concentrations of H^+ quencher added to the 17 mM iodide solutions are (a) 0.0, (b) 2.5, (c) 8.0, and (d) 27 mM. Spectrum e is the probe-only Raman spectrum of the aqueous I^- solution. All spectra are shown without offset. Inset: normalized electron fluorescence at 12640 cm^{-1} (Raman shift = 2000 cm^{-1}) (◆) and normalized enhanced bend area (●), as a function of $[H^+]$. Least-squares fits to the fluorescence and bend area decays are single-exponential curves with decay constants 150 M^{-1} and 134 M^{-1}, respectively. The standard deviation of the exponential factor is 5%.

The other experimental conditions that affect the Raman bend enhancement and fluorescence intensity are the concentration of parent anions, pump power, and probe power. Figure 3 shows that the *ratio* of the bend area and fluorescence integrated from 1400 to 1800 cm^{-1} *remains constant as all three experimental conditions are varied*. The spectral correlation is consistent with the conclusion that both the Raman bend enhancement and the fluorescence have the same molecular origin, namely the solvated electron. Although not evident from the figure, it is important to note that both spectral features were found to scale linearly with the 683 nm probe powers.

3.3. NIR Emission of the Solvated Electron. Figure 4 presents the scanned emission spectra of solvated electrons in D_2O (a) and H_2O (b). These spectra were obtained following steps similar to the processing of the CCD data. One significant difference is the negligible pump-only background (not shown) of the scanning experiment, due to the gated selection of the signal due to the probe pulse; therefore, subtraction of the pump-only component is unnecessary. The instrument sensitivity correction is done as for the CCD data, but the scanned spectra includes an additional correction for the collection lens chromatic aberration over the range 900−1600 nm as explained above. Finally, we note that corrections for the attenuation of the bulk water scattering in the pump + probe spectrum (~15%)

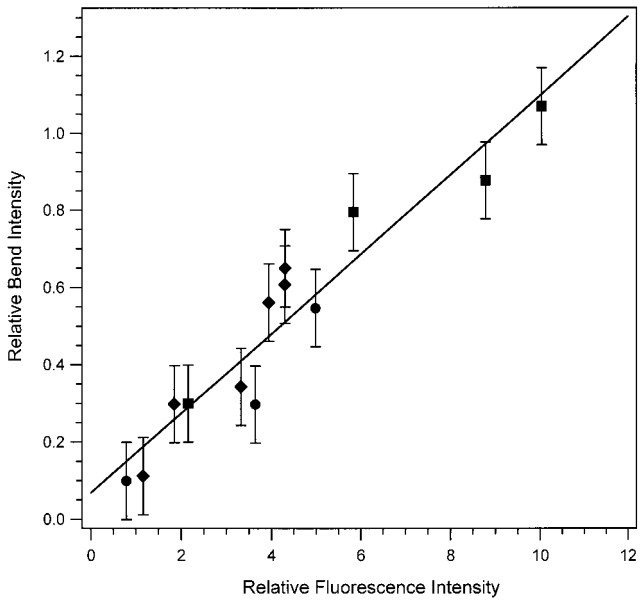

Figure 3. Correlation of the hydrated electron resonance Raman integrated bend intensity with the fluorescence emission integrated beneath the bend mode from 13 240 to 12 840 cm^{-1} (Raman shift = 1400−1800 cm^{-1}). Constant 218 nm pump (1.8 mW) and 683 nm probe (2.0 mW) powers, with I^- concentrations varying from 0.77 to 49 mM (◆). Constant probe power (2.0 mW) and I^- concentration (7 mM) with pump powers varying from 0.25 to 2.4 mW (■). Constant pump power (2.6 mW) and I^- concentration (7.7 mM) with probe powers varying from 0.3 to 2.2 mW (●). The least-squares linear fit (R = 0.95) indicates the nearly constant ratio of bend enhancement to fluorescence.

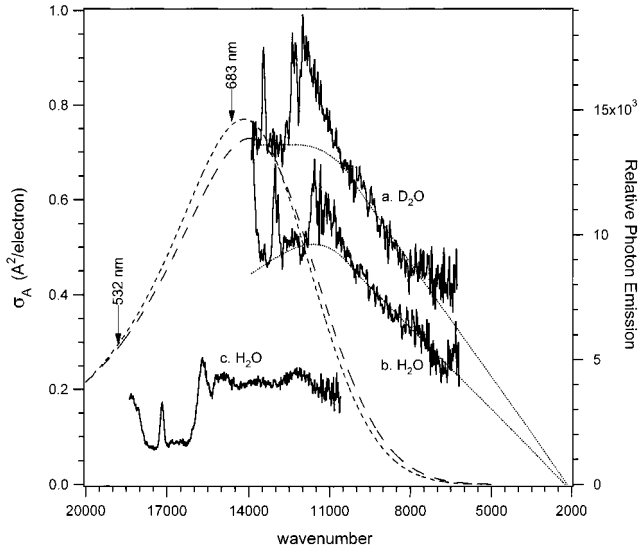

Figure 4. Combined fluorescence and Raman emission spectra of the solvated electron with 683 nm excitation in D_2O (a) and H_2O (b) and with 532 nm excitation in H_2O (c). Relative scaling of spectra obtained with 683 nm excitation and with 532 nm excitation are determined by comparing the integrated intensity of the water Raman stretch band of the component (pump + probe)−(pump) spectra (not shown). Spectra (a−c) are corrected for the instrument response, and emission intensities shown are proportional to the number of photons detected for a constant energy band-pass. Spline-polynomial fits to the fluorescence with 683 excitation are shown with linear extrapolation (···). Absorption cross-sections for the hydrated electron in H_2O (− − −) and D_2O (- - -) are shown for comparison.[46]

and self-absorption (∼10% change across the full spectrum) were modeled as for the 532 nm data. These minor corrections are included in the spectra of Figure 4.

A much more significant change in the emission data presented in Figure 4 is the multiplication of all spectra (including the 532 nm probe data) by a factor proportional to λ^2, which converts the spectral intensities from constant *wavelength* band-pass to constant *energy* band-pass. This adjustment produces spectral profiles that accurately depict the relative emission quantum efficiency in various spectral regions[48] and is especially important for our broad emission spectra. The result is a relative increase in emission intensity at 1600 nm that is more than three times greater than the increase at 900 nm, thus accentuating the remarkable breadth of the fluorescence emission from solvated electrons in H_2O and D_2O.

The fluorescence curves shown in Figure 4 are determined by a spline fit to the background beneath the sharper Raman features prominent in the water bend, stretch, and stretch + librational combination band regions. Confirmation of the partitioning of the emission is provided by noting that the emission above the fluorescence curves show significant frequency displacement upon isotopic substitution, as expected for these Raman modes. The low-energy limits of the fluorescence emission are beyond the cutoff of the PMT. An approximate linear extrapolation of the decaying fluorescence spectra indicates that the emission could extend to 2000 cm^{-1} (5 μm) for both $e^-(H_2O)$ and $e^-(D_2O)$. Note that an extrapolated fit based on the mirror reflection of the absorption spectrum would be incorrect, since the high-energy side of the absorption spectrum is caused by excitation from deep traps[15] or transitions to higher electronic states[46] rather than a vibrational progression.

3.4. 683 nm Fluorescence Quantum Yield. The water Raman stretch is a reliable internal standard which can be used to quantify weak fluorescence emission yields.[49] The fluorescence emission quantum yield of the solvated electron in H_2O excited at 683 nm can be expressed in terms of the water Raman stretch cross section,[49] and the 683 nm absorption cross-section of the electron $\sigma^e_{abs} = 0.71$ Å^2 by

$$\Phi = \frac{\sigma^w_{Ram} I^e_{fl} c^w}{\sigma^e_{abs} I^w_{Ram} c^e} \Delta \qquad (1)$$

where I^e_{fl} is the integrated electron fluorescence intensity, I^w_{Ram} is the integrated Raman stretch intensity, the bulk water concentration $c^w = 55$ M and the electron concentration c^e = 0.25 mM. The factor Δ depends on the relative depolarization ratios of the Raman and fluorescence emission and is nearly unity.[37] The resulting quantum yield for emission *in our spectral window* is 5.3×10^{-7}. This value should be considered a lower limit on the fluorescence quantum yield of the solvated electron in H_2O. If emission is assumed to decay linearly toward 5 μm, Φ increases slightly to 6.0×10^{-7}; an additional linear extrapolation to 683 nm on the high energy side gives $\Phi = 6.5 \times 10^{-7}$. If the fluorescence were to deviate significantly from a linear decay toward 5 μm, the strongly decreasing probability of emitting NIR photons (ω^3 factor of the Einstein A-coefficient) would diminish the effect of this change on the total integrated fluorescence area, thus Φ is unlikely to differ significantly from the 6.5×10^{-7} value reported here.

The fluorescence quantum yield of the electron in D_2O exceeds that in H_2O by a factor of 1.4 ± 0.1, as determined by the ratio of the measured (not extrapolated) fluorescence emission, the ratio of electron concentrations, and the relative absorption coefficients at 683 nm. This ratio of deuterated and hydrated electron fluorescence is likely insensitive to the unmeasured fluorescence.

3.5. Strickler−Berg Analysis. Absorption and fluorescence spectra of the solvated electron can be utilized to calculate the natural radiative lifetime τ_r of the aqueous electron according to the Strickler−Berg relationship[50]

$$\tau_r^{-1} = 2.88 \times 10^{-9} n^2 \langle \nu_f^{-3} \rangle_{Av}^{-1} \frac{g_l}{g_u} \int \epsilon \, d(\ln \nu) \qquad (2)$$

where $n = 1.33$ is the index of refraction, g_l and g_u are the respective degeneracies of the ground state and excited state, ϵ is the molar decadic absorption coefficient, and ν is frequency (cm^{-1}). The term $\langle \nu_f^{-3} \rangle_{Av}^{-1}$ is calculated from the integrals of the fluorescence photon intensity $I_f(\nu)$ as

$$\langle \nu_f^{-3} \rangle_{Av}^{-1} = \int I_f(\nu) \, d\nu \Big/ \int \frac{I_f(\nu) \, d\nu}{\nu^3} \qquad (3)$$

The degeneracy of the ground electronic s-state is 1. The excited state manifold consists of three p-states that likely interconvert on the picosecond time scale,[22,51] but are nondegenerate on the time scale of absorption and fluorescence processes (see below). Therefore $g_l = g_u = 1$. The resulting radiative lifetime calculated using the extrapolated fluorescence curves is ∼40 ns. The uncertainty in the decay time is due primarily to the strong dependence of the $\langle \nu_f^{-3} \rangle_{Av}$ factor on the profile of the fluorescence spectrum toward low ν.[52]

3.6. Rate of Fluorescence Quenching. The time scale τ for the decay of the emission is related to the quantum yield Φ using the kinetic expression

$$\Phi = \tau / \tau_{rad} \qquad (4)$$

Using the estimated ∼40 ns determined from the extrapolated curves, and the corresponding 6.5×10^{-7} quantum yield, $\tau =$ ∼30 fs. The 1.4-fold greater quantum yield for $e^-(D_2O)$ results in an ∼40 fs lifetime.

3.7. Resonance Raman Cross Sections. The cross sections of the enhanced Raman bands can be quantified using the water Raman stretch of the probe-only spectrum as an internal standard.[49] From the ratios of the integrated areas of the solvated electron features relative to the water stretch and the ratio of electron concentration relative to 55 M bulk water, the 532 nm $e^-(H_2O)$ Raman cross-section are as follows (in units Å²/electron): $>5 \times 10^{-9}$ (libration); $(1.3 \pm 0.2) \times 10^{-9}$ (bend), and $(3 \pm 1) \times 10^{-9}$ (stretch). For 683 nm excitation the cross sections are $(3.8 \pm 0.2) \times 10^{-9}$ (bend) and $(3 \pm 1) \times 10^{-9}$ (stretch).

4. Discussion

We present here the first measurement of the spontaneous Raman and fluorescence emission spectra and fluorescence quantum yield for the aqueous solvated electron. In overview, we observe strong resonance enhancement of the water Raman libration and intramolecular bands. A broad fluorescence emission from the solvated electron extends from 720 nm to beyond 1600 nm with a quantum yield of $\sim 6.5 \times 10^{-7}$. A near-IR radiative lifetime of ∼40 ns results in an effective fluorescence lifetime of ∼30 fs based on our viewing window. The fluorescence increases by a factor of ∼1.4 in D_2O, implying an increased lifetime of ∼40 fs. We now discuss these observations in reference to the relevant literature.

4.1. Resonance Raman Spectra. The remarkable resonance Raman features will be analyzed more quantitatively in a subsequent manuscript so only the salient points are summarized here.[53] The resonantly enhanced frequencies of the solvated electron Raman spectra provide vibrational data on the ground state structure of water molecules in immediate proximity with the electron. The idea that the electron simply perturbs the hydrogen bond network of bulk water is inconsistent with the shift of *both* bend and stretch modes to frequencies *lower* than their counterparts in bulk water. These frequencies should move in opposite direction for a change in hydrogen bond strength.[54] An alternative possibility is that donation of the solvated electron charge density into unoccupied Rydberg orbitals of proximal water molecules causes a slight weakening of the OH bonds and therefore decreased internal vibrational frequencies.

The resonance Raman enhancements indicate substantial increases in the scattering cross-sections of individual water molecules due to significant coupling of the water libration and intramolecular modes to the s→p transition. Assuming that six water molecules are the primary contributors to the scattering of each solvated electron,[3,55] the 683 nm cross-sections reflect enhancement factors of ∼2000-fold for the stretch, and ∼300000-fold for the bend. Such couplings of a solute electronic transition to solvent modes have not been observed before, and were largely unpredicted in MD simulations of the solvated electron.[56] The strongly enhanced libration is in agreement with coherences observed in the fastest pump−probe and photon echo experiments of the hydrated electron.[7,57,58]

4.2. Fluorescence Emission. The enormous breadth of the fluorescence emission, the blue-shift upon excitation with 532 nm, and the lack of an obvious emission peak clearly indicate that the fluorescence originates from an *unrelaxed* excited state. The Strickler−Berg formula has been used successfully to characterize such unrelaxed emission[37,59] in addition to the original application to fully relaxed systems.[50] Similarly, we employ it here to estimate the increase in natural radiative lifetime caused by the significant red-shift in fluorescence emission relative to the absorption spectrum. The resulting 40 ns near-IR radiative lifetime is based primarily on the observed 720−1600 nm emission, with a conservative linear extrapolation to 5 μm to account for the emission at lower energy. The 30 fs decay time derived from the near-IR radiative lifetime and fluorescence quantum yield should not be considered the fluorescence or T_1 lifetime of the fully relaxed excited state of the aqueous solvated electron. Instead this ultrafast decay time is best described as the *effective* fluorescence lifetime based on our near-IR viewing window.

One mechanism that could conceivably cause the ultrafast fluorescence decay is internal conversion. This hypothesis is not without precedent; similar rates were proposed for rapid curve crossings upon photoexcitation of cycloalkenes, based upon fluorescence quantum yields that were nearly as low as that determined for the solvated electron.[35,36] The rapidity of the $1B_2-2A_1$ nonadiabatic transition in pericyclic ring-opening reactions is undoubtedly facilitated by the close energetic proximity of the excited states, so that the transition occurs with a minimum of vibrational excitation. However, calculations of the solvated electron do not show evidence of an optically dark state in close proximity with the optically allowed p-states.[4] It is therefore unlikely that a dynamic curve crossing can account for the short fluorescence lifetime of the solvated electron.

The similarity of the isotope effects in the fluorescence and phosphorescence quantum yields noted for a variety of aromatic molecules to the isotope effect measured in this work suggests that these systems might provide an insight into the nature of the ultrafast fluorescence decay of the solvated electron. The increased emission upon deuteration of aromatics results from a decreased rate of nonradiative transitions, due to the higher

vibrational quantum number of the final states.[60,61] However, the nonradiative processes that compete with fluorescence in aromatic molecules have time constants of ~10 ns, which serves to reinforce the qualitative picture that transfer of large amounts of electronic energy to a set of highly excited ground-state vibrations is likely much slower than the 30−40 fs decay rate observed here.

The most likely explanation for the fluorescence decay is a mechanism in which the rate of solvation (defined qualitatively by a rate k_{solv}) exceeds the rate of internal conversion k_{ic}. This hypothesis is supported by the measurement of fluorescence emission to 1.6 μm. Such low energy emission would be improbable if the relaxation process were truncated by a much faster internal conversion. Since the electrons remain in the excited p-state during solvation, how is it possible to explain the low fluorescence quantum yield? The most likely answer is that the fluorescence observed in our 700−1600 nm window is quenched via very rapid relaxation that sweeps the emission wavelength beyond our reddest detection limit. This picture helps define k_{solv}: it is the rate at which we lose the ability to measure photon emission due to the shift beyond 1.6 μm.

The isotope effect is readily explained in the model of rapid solvation. Our data are consistent with a solvation mechanism that occurs along rotational and in part intramolecular coordinates for at least 30 fs after photoexcitation. The molecular motion accounting for a 20−40 fs decay is in the inertial regime.[62,63] The inertial rotations are $\sqrt{2}$ slower in D_2O causing a decrease in the rate of the dynamic Stokes shift across the 700−1600 window, and a proportional increase in the emission time from the deuterated system. Our results are consistent with femtosecond transient absorption and photon echo experiments in which an ~50 fs Gaussian relaxation rate and coherence features[7,57,58] show the same isotope effect as ours and were similarly interpreted in terms of underdamped rotational motion.

The dominant contribution of rotational motion to the fastest solvation processes in water[64] was first predicted in simulations[65] and was later confirmed in experimental studies of molecular solutes.[66] The fact that the initial relaxation of the p-state solvated electron should show a 1.4 isotope effect was successfully modeled in one MD simulation[67] and in a recent instantaneous normal-mode analysis.[68] Other simulations and theory have emphasized the importance of translational motion and mechanical expansion for the fastest relaxation in water,[11,17,69−71] particularly for solutes that enlarge significantly upon photoexcitation as expected for the solvated electron. Since the mass of D_2O is only 11% higher than H_2O, these models show isotope effects in the initial solvation process that are less than 80% of the value of 1.4 determined from our experiments. Our data do not preclude the possibility of significant relaxation due to translations, however these modes must *follow* the inertial librations, and cannot contribute significantly to the ~1 eV relaxation monitored in our spectral window.

The calculated stimulated emission cross-sections in the MD calculations of Schwartz and Rossky[14,72] prompted us to model the stimulated emission corresponding to our spontaneous emission spectra. This transformation highlights the molecular dipole coupling between ground and excited states, since the Einstein A-coefficient includes a factor of ω^3 that is due to the intrinsic decrease in the radiation density of states toward longer wavelengths:

$$A(\mathrm{p}\rightarrow\mathrm{s}) = \frac{4}{3\hbar}\left(\frac{\omega}{c}\right)^3 |\mu_{sp}|^2 \qquad (5)$$

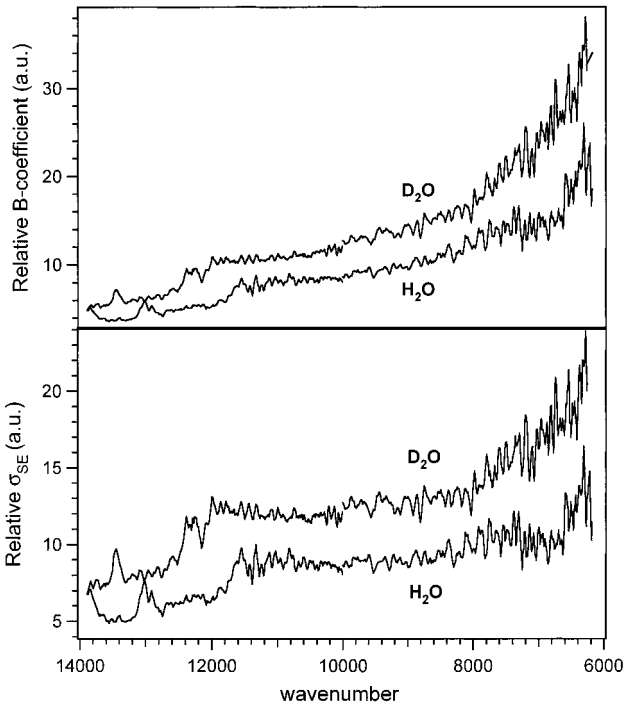

Figure 5. (Upper) Calculated spectral *B*-coefficients for the solvated electron in D_2O and H_2O. The two traces were obtained by a scaled division of the 683 nm spontaneous emission curves (a, b of Figure 4) by ω^3. (Lower) Stimulated emission cross-sections obtained by multiplying the spectral *B*-coefficients by ω.

where μ_{sp} is the transition dipole moment connecting the initial (p) and final (s) states. On the other hand, the only molecular property that affects the Einstein *B*-coefficient is μ_{sp}:

$$B(\mathrm{p}\rightarrow\mathrm{s}) = \frac{2\pi}{3\hbar^2}|\mu_{sp}|^2 \qquad (6)$$

Our photon fluorescence emission is directly related to an effective time-integrated spectral *A*-coefficient and can be converted to a spectral *B*-coefficient by a division by ω^3 (Figure 5). The stimulated emission cross section is obtained via multiplication of the spectral *B*-coefficient by ω.[73] Both the spectral *B*-coefficient and modeled stimulated emission cross-section increase toward longer wavelength as shown in Figure 5. The result shows that our measured declining fluorescence is due to the inherent decrease of the probability of spontaneously emitting NIR photons, rather than a reduction in the transition dipole coupling. MD simulations support this observation in calculating an increased transition dipole after photoexcitation on both the ~25 and 300 fs time scales, due to the rapid increase in excited-state charge distribution.[67]

Within the framework of a rapid solvation model, the increase in the near-IR stimulated emission cross section shown in Figure 5 could be due to two possibilities. One is that the spontaneous (and therefore stimulated) emission toward 1.6 μm includes a component from the high-energy wing of the *relaxed* p-state electrons whose peak emission is beyond the low energy cutoff of the detector. Our observation of the 1.4-fold isotope effect argues against this possibility in view of the isotope independent p→s transition rate supported by femtosecond transient absorption experiments and MD simulations.[7,56] A better explanation is that the rate of the emission red-shift decreases as solvation occurs, leading to a relatively longer duration for spontaneous emission at longer wavelengths and a corresponding increase in calculated stimulated emission cross-section. The hypothesis

of a slowing dynamic Stokes-shift is qualitatively consistent with MD simulations of the ultrafast relaxation of the excited-state solvated electron. Calculations of the evolving stimulated emission spectra show a rapid (∼25 fs) Stokes shift toward an emission peak that is 60% of the resonant excitation energy followed by a slower (hundreds of femtoseconds) shift toward a peak that is 30% of the excitation energy.[14,72] The magnitude of the fast shift of the simulation is possibly insufficient to fully explain the extremely low quantum yield determined experimentally; however, it is difficult to make a quantitative comparison since the simulated spectra were convoluted with a 100 or 300 fs instrument response.[14,72] Also, there is clearly emission beyond our detection cutoff that is critical for modeling the full stimulated emission profile.

The fluorescence data presented here leave unanswered many important questions about the solvation process. Aside from the isotope effect, which implicates rotational or possibly intramolecular motion along the initial solvation coordinate, the fluorescence data do not indicate the relative portion of the relaxation due to the various isotope-dependent modes. From the resonance Raman intensities measured as low as 400 cm^{-1}, a significant fraction of the observed ∼8000 cm^{-1} Stokes shift (10−20%) is caused by solvent reorganization along librational and intramolecular (bend and stretch) coordinates.[53] The remaining relaxation occurs along isotope-sensitive coordinates but on a time scale apparently longer than the dephasing that dampens resonance Raman intensities. The inclusion of a frictionally damped generalized solvation coordinate will allow self-consistent treatment of both fluorescence and resonance Raman spectra and provide some insight into the energy distribution along seen and unseen solvent coordinates.[74−77]

We conclude by noting that the observation of fluorescence from the solvated electron in aqueous solution over a very broad range of wavelengths into the near-IR supports the model of an ultrafast solvation process that exceeds the rate of internal conversion. A significant part of the solvation occurs in ∼30 fs, as shown by the extremely low quantum yield of fluorescence in a window that allows detection of emission with energy as low as ∼40% of the excitation photons. Rotational modes are primarily responsible for the ∼8000 cm^{-1} Stokes shift as shown by the strong resonance Raman enhancement and significant isotope effect on the fluorescence quantum yield. These resonance Raman and fluorescence emission spectra provide new data on mode specific electron−solvent coupling and relaxation that will help elucidate the structure and dynamics of the aqueous solvated electron.

Acknowledgment. We appreciate many stimulating discussions with Judy Kim and Dave McCamant, and thank Steven Bradforth for constructive comments on the manuscript. Hamamatsu Inc. (Matt Matsumoto) is thanked for providing the NIR PMT system. This work was supported by NSF Grant CHE 98 01651.

References and Notes

(1) Hart, E. J.; Boag, J. W. *J. Am. Chem. Soc.* **1962**, *84*, 4090.
(2) Schindewolf, U. *Angew. Chem., Int. Ed. Engl.* **1978**, *17*, 887−901.
(3) Schlick, S.; Narayana, P. A.; Kevan, L. *J. Chem. Phys.* **1976**, *64*, 3153−3160.
(4) Feng, D.-F.; Kevan, L. *Chem. Rev.* **1980**, *80*, 1−20.
(5) Schnitker, J.; Rossky, P. J. *J. Chem. Phys.* **1987**, *86*, 3471−3485.
(6) Silva, C.; Walhout, P. K.; Yokoyama, K.; Barbara, P. F. *Phys. Rev. Lett.* **1998**, *80*, 1086−1089.
(7) Yokoyama, K.; Silva, C.; Son, D. H.; Walhout, P. K.; Barbara, P. F. *J. Phys. Chem. A* **1998**, *102*, 6957−6966.
(8) Kimura, Y.; Alfano, J. C.; Walhout, P. K.; Barbara, P. F. *J. Phys. Chem.* **1994**, *98*, 3450−3458.
(9) Assel, M.; Laenen, R.; Laubereau, A. *J. Phys. Chem. A* **1998**, *102*, 2256−2262.
(10) Assel, M.; Laenen, R.; Laubereau, A. *Chem. Phys. Lett.* **2000**, *317*, 13−22.
(11) Schwartz, B. J.; Rossky, P. J. *J. Chem. Phys.* **1994**, *101*, 6902−6916.
(12) Long, F. H.; Lu, H.; Eisenthal, K. B. *Phys. Rev. Lett.* **1990**, *64*, 1469−1472.
(13) Shi, X.; Long, F. H.; Lu, H.; Eisenthal, K. B. *J. Phys. Chem.* **1996**, *100*, 11903−11906.
(14) Schwartz, B. J.; Rossky, P. J. *J. Chem. Phys.* **1994**, *101*, 6917−6926.
(15) Romero, C.; Jonah, C. D. *J. Chem. Phys.* **1989**, *90*, 1877−1887.
(16) Rossky, P. J.; Schnitker, J. *J. Phys. Chem.* **1988**, *92*, 4277−4285.
(17) Schwartz, B. J.; Rossky, P. J. *J. Mol. Liq.* **1995**, *65/66*, 23−30.
(18) Wallqvist, A.; Martyna, G.; Berne, B. J. *J. Phys. Chem.* **1988**, *92*, 1721−1730.
(19) Borgis, D.; Bratos, S. *J. Mol. Struct.* **1997**, *436−437*, 537−541.
(20) Bratos, S.; Leicknam, J.-C.; Borgis, D.; Staib, A. *Phys. Rev. E* **1997**, *55*, 7217−7227.
(21) Barnett, R. N.; Landman, U.; Rajagopal, G.; Nitzan, A. *Isr. J. Chem.* **1990**, *30*, 85−105.
(22) Schnitker, J.; Motakabbir, K.; Rossky, P. J.; Friesner, R. *Phys. Rev. Lett.* **1988**, *60*, 456−459.
(23) Kestner, N. R. In *Electrons in Fluids*; Jortner, J., Kestner, N. R., Eds.; Springer-Verlag: Berlin, 1973; pp 1−28.
(24) Copeland, D. A.; Kestner, N. R.; Jortner, J. *J. Chem. Phys.* **1970**, *53*, 1189.
(25) Myers, A. B.; Mathies, R. A. In *Biological Applications of Raman Spectrometry: Resonance Raman Spectra of Polyenes and Aromatics*; Spiro, T. G., Ed.; John Wiley & Sons: New York, 1987; Vol. 2; pp 1−58.
(26) Waterland, M. R.; Kelley, A. M. *J. Chem. Phys.* **2000**, *113*, 6760−6773.
(27) Myers, A. B. *Annu. Rev. Phys. Chem.*; Annual Reviews, Inc.: Palo Alto, 1998; Vol. 49; pp 267−295.
(28) Worlock, J. M.; Porto, S. P. S. *Phys. Rev. Lett.* **1965**, *15*, 697−699.
(29) Smith, B. L.; Koehler, W. H. *J. Phys. Chem.* **1973**, *77*, 1753−1758.
(30) White, T. R.; Glaunsinger, W. S. *J. Phys. Chem.* **1975**, *79*, 2942−2947.
(31) De Bettignies, B.; Lelieur, J. P. *J. Phys. Chem.* **1981**, *85*, 1014−1016.
(32) Kulinowski, K.; Gould, I. R.; Myers, A. B. *J. Phys. Chem.* **1995**, *99*, 9017−9026.
(33) Cao, X.; McHale, J. L. *J. Chem. Phys.* **1998**, *109*, 1901−1911.
(34) Bardeen, C. J.; Rosenthal, S. J.; Shank, C. V. *J. Phys. Chem. A* **1999**, *103*, 10506−10516.
(35) Reid, P. J.; Lawless, M. K.; Wickham, S. D.; Mathies, R. A. *J. Phys. Chem.* **1994**, *98*, 5597−5606.
(36) Lawless, M. K.; Wickham, S. D.; Mathies, R. A. *Acc. Chem. Res.* **1995**, *28*, 493−502.
(37) Kochendoerfer, G. G.; Mathies, R. A. *J. Phys. Chem.* **1996**, *100*, 14526−14532.
(38) Mokhtari, A.; Chesnoy, J.; Laubereau, A. *Chem. Phys. Lett.* **1989**, *155*, 593−598.
(39) de Boeij, W. P.; Pshenichnikov, M. S.; Wiersma, D. A. *J. Phys. Chem.* **1996**, *100*, 11806−11823.
(40) Book, L. D.; Scherer, N. F. *J. Chem. Phys.* **1999**, *111*, 792−795.
(41) Larsen, D. S.; Ohta, K.; Xu, Q.; Cyrier, M.; Fleming, G. R. *J. Chem. Phys.* **2001**, *114*, 8008−8039.
(42) Blandamer, M. J.; Fox, M. F. *Chem. Rev.* **1970**, *70*, 59.
(43) Kloepfer, J. A.; Vilchiz, V. H.; Lenchenkov, V. A.; Bradforth, S. E. in *Liquid Dynamics: Into the New Millenium*; Fourkas, J., Ed.; American Chemical Society: Washington, DC, 2001; pp 1−17.
(44) Shirom, M.; Stein, G. *J. Chem. Phys.* **1971**, *55*, 3372−3378.
(45) Shirom, M.; Stein, G. *J. Chem. Phys.* **1971**, *55*, 3379−3382.
(46) Jou, F. Y.; Freeman, G. R. *J. Phys. Chem.* **1979**, *83*, 2383−2387.
(47) Jonah, C. D.; Miller, J. R.; Matheson, M. S. *J. Phys. Chem.* **1977**, *81*, 931−934.
(48) Calvert, J. G.; Pitts, J. N. *Photochemistry*; John Wiley: New York, 1966.
(49) Champion, P. M.; Lange, R. *J. Chem. Phys.* **1980**, *73*, 5947−5957. The absolute Raman cross-sections of the water stretch are extrapolated from the measured 514.5 nm value of 8.5×10^{-13} A^2/molecule by assuming a scattering cross-section proportional to $\nu_S^3\nu_L$, where ν_S and ν_L are the respective frequencies of the scattered and laser light. The extrapolated cross-sections are 7.3×10^{-13} A^2/molecule (532 nm) and 2.2×10^{-13} A^2/molecule (683 nm).
(50) Strickler, S. J.; Berg, R. A. *J. Chem. Phys.* **1962**, *37*, 814−822.
(51) Reid, P. J.; Silva, C.; Walhout, P. K.; Barbara, P. F. *Chem. Phys. Lett.* **1994**, *228*, 658−664.

(52) As an example, if the extrapolated emission from 1.6 to 5 μm were omitted, the radiative lifetime decreases to 22 ns. The value based on the extrapolated emission is likely a more accurate lower limit.

(53) Tauber, M. J.; Mathies, R. A. *Chem. Phys. Lett.*, submitted.

(54) Pimentel, G. C.; McClellan, A. L. *The Hydrogen Bond*; Freeman: San Francisco, 1960.

(55) Narayana, P. A.; Bowman, M. K.; Kevan, L.; Yudanov, V. F.; Tsvetkov, Y. D. *J. Chem. Phys.* **1975**, *63*, 3365−3371.

(56) Schwartz, B. J.; Rossky, P. J. *J. Chem. Phys.* **1996**, *105*, 6997−7010.

(57) Emde, M. F.; Baltuska, A.; Kummrow, A.; Pshenichnikov, M. S.; Wiersma, D. A. *Phys. Rev. Lett.* **1998**, *80*, 4645−4648.

(58) Kummrow, A.; Emde, M. F.; Baltuska, A.; Pshenichnikov, M. S.; Wiersma, D. A. *J. Phys. Chem. A* **1998**, *102*, 4172−4176.

(59) Shreve, A. P.; Trautman, J. K.; Owens, T. G.; Albrecht, A. C. *Chem. Phys. Lett.* **1991**, *178*, 89−96.

(60) Robinson, G. W.; Frosch, R. P. *J. Chem. Phys.* **1962**, *37*, 1962−1973.

(61) Abramson, A. S.; Spears, K. G.; Rice, S. A. *J. Chem. Phys.* **1972**, *56*, 2291−2308.

(62) Carter, E. A.; Hynes, J. T. *J. Chem. Phys.* **1991**, *94*, 5961−5979.

(63) Maroncelli, M. *J. Mol. Liq.* **1993**, *57*, 1−37.

(64) Fleming, G. R.; Cho, M. *Annu. Rev. Phys. Chem.*; Annual Reviews Inc.: Palo Alto, 1996; Vol. 47; pp 109−135.

(65) Maroncelli, M.; Fleming, G. R. *J. Chem. Phys.* **1988**, *89*, 5044−5069.

(66) Jimenez, R.; Fleming, G. R.; Kumar, P. V.; Maroncelli, M. *Nature* **1994**, *369*, 471−473.

(67) Barnett, R. N.; Landman, U.; Nitzan, A. *J. Chem. Phys.* **1989**, *90*, 4413−4422.

(68) Yang, C.; Wong, K. F.; Skaf, M. S.; Rossky, P. J. *J. Chem. Phys.* **2001**, *114*, 3598−3611.

(69) Nandi, N.; Roy, S.; Bagchi, B. *J. Chem. Phys.* **1995**, *102*, 1390−1397.

(70) Stratt, R. M.; Maroncelli, M. *J. Phys. Chem.* **1996**, *100*, 12981−12996.

(71) Berg, M. A. *J. Chem. Phys.* **1999**, *110*, 8577−8588.

(72) Schwartz, B. J.; Rossky, P. J. *J. Phys. Chem.* **1995**, *99*, 2953−2958.

(73) Craig, D. P.; Thirunamachandran, T. *Molecular Quantum Electrodynamics*; Academic Press: 1984. The factor of ω results from the units of the *B*-coefficient [$m^3/(J\ s^2)$]. The derivation of the energy-independent extinction coefficient (or cross section) requires multiplication of the *B*-coefficient by hω to cancel the energy term in the denominator.

(74) Yan, Y. J.; Mukamel, S. *J. Chem. Phys.* **1987**, *86*, 6085−6107.

(75) Mukamel, S. *Adv. Chem. Phys.*; John Wiley and Sons: New York, 1988; Vol. 70; pp 165−230.

(76) Li, B.; Johnson, A. E.; Mukamel, S.; Myers, A. B. *J. Am. Chem. Soc.* **1994**, *116*, 11039−11047.

(77) Myers, A. B. *Chem. Phys.* **1994**, *180*, 215−230.